To: Structural Health Monitoring

Sparse damage detection via the elastic net method using modal data

Rongrong Hou
School of Civil Engineering,
Harbin Institute of Technology, China
rongrong.hou@connect.polyu.hk

Xiaoyou Wang
Department of Civil and Environmental Engineering,
The Hong Kong Polytechnic University,
Kowloon, Hong Kong, P. R. China
xiaoyou.wang@connect.polyu.hk

Yong Xia*
Professor,
[1] Department of Civil and Environmental Engineering,
The Hong Kong Polytechnic University,
Kowloon, Hong Kong, P. R. China
ceyxia@polyu.edu.hk

[2] School of Civil and Hydraulic Engineering,
Huazhong University of Science and Technology,
Wuhan, Hubei, P. R. China

(*Corresponding author)

Abstract

The l_1 regularization technique has been developed for damage detection by utilizing the sparsity feature of structural damage. However, the sensitivity matrix in the damage identification exhibits a strong correlation structure, which does not suffice the independency criteria of the l_1 regularization technique. This study employs the elastic net method to solve the problem by combining the l_1 and l_2 regularization techniques. Moreover, the proposed method enables the grouped structural damage being identified simultaneously, whereas the l_1 regularization cannot. A numerical cantilever beam and an experimental three-story frame are utilized to demonstrate the effectiveness of the proposed method. The results showed that the proposed method is able to accurately locate and quantify the single and multiple damages, even when the number of measurement data is much less than the number of elements. In particular, the present elastic net technique can detect the grouped damaged elements accurately, whilst the l_1 regularization method cannot.

1. Introduction

Vibration-based structural damage identification has received much attention over the last decades. Numerous methods have been developed using structural vibration characteristics [1-3]. Doebling et al. [4] and Sohn et al. [5] present a comprehensive review of vibration-based damage detection methods before 1996 and between 1996 and 2001, respectively. Recently, a number of advanced methods based on signal processing techniques [6-8] and machine learning [9-11] have been proposed. Moreover, researchers have developed various techniques to consider the uncertainties and temperature effects for reliable damage detection [12, 13]. Several literature surveys review the new development of damage identification for civil engineering structures [14-16].

Structural damage identification is essentially an inverse problem and is typically ill-posed. Moreover, as the number of available vibration measurements is usually less than that of structural elements, such identification is an underdetermined problem in mathematics. Most previous vibration-based damage detection methods employ the Tikhonov regularization (or l_2 regularization) to deal with these problems [17, 18]. The l_2 regularization has a closed-form solution and tractable methods for choosing the regularization parameter, and thus is efficient and convenient for implementation [19, 20]. However, the main drawback of the l_2 regularization is that it tends to produce over-smooth solutions [21]. Consequently, the identified damage is distributed to many structural elements. This is not consistent with the practical situation that damage usually occurs in a few sections or members only especially at the early stage.

Structural damage possesses sparsity compared with all elements of the entire structure, which is an important prior information that can be exploited for more accurate damage identification. According to the sparse recovery theory, the l_1 regularization technique can not only deal with underdetermined problems, but also favor sparsity in the solutions [21]. In this

regard, some researchers (including the authors) used the l_1 regularization technique for damage detection [22-27]. Although the l_1 regularization technique has achieved excellent performance in many applications, it has some limitations. For example, the l_1 regularization technique is essentially designed for selecting individual variables. If there is a group of highly correlated variables, it typically only selects a single variable from the group that is the most correlated with the residual [28]. Moreover, the sensing matrix of l_1-regularized problems should suffice certain independency criteria to ensure the exact recovery of the unknown vector [21]. For the sensitivity-based damage identification, the sensitivity matrix serves as the sensing matrix while the columns are almost linearly dependent. Once the independence criteria are not satisfied, the solution may become unstable and suboptimal [29, 30].

Some researchers compared the performances of l_1 and l_2 regularization techniques and found that neither of them uniformly dominates the other [31, 32]. Xu et al. [33] pointed out that sparsity and algorithmic stability contradict with each other, i.e., a sparse algorithm cannot be stable and vice versa. In particular, the l_1 regularization technique cannot be stable, while the l_2 regularization technique has strong stability property and is therefore not sparse. Given that sparsity and stability are both desirable properties, an appropriate algorithm should be designed to achieve a trade-off between these two properties. To this end, Zou and Hastie [34] proposed a new regularization method, i.e., the elastic net, which combines the l_1 and l_2 regularization techniques to get the best of both worlds.

The elastic net is able to enforce sparsity in the solution as the l_1 regularization technique does, while enjoying a similar stable behavior of the l_2 regularization. Moreover, the elastic net encourages the grouping effect that grouped variables are able to be selected together. Consequently, compared with the l_1 regularization, the elastic net enables the structure of interest to be modeled with a larger number of elements such that the local damage is directly modeled and quantified. For the l_1-regularized problem, the ratio of the number of unknown

parameters to that of the measurements may significantly affect the accuracy and convergence of the results [21]. The elastic net has been verified to be more effective when the number of unknowns is much larger than that of measurements, in comparison to the l_1 regularization technique [34].

The previous vibration-based damage detection methods either utilize l_2 regularization or l_1 regularization only. This study takes advantage of the strengths of both regularization techniques via the elastic net algorithm, which is introduced to structural damage identification for the first time. An iterative damage detection technique is proposed through incorporating the elastic net method into the sensitivity-based model updating. The proposed method improves the condition of the sensitivity matrix and thus resolves the instability and divergence problems in damage identification. Numerical and experimental studies demonstrate the effectiveness and superiorities of the proposed method.

2. Elastic Net Algorithm

Consider a linear model

$$y = X\theta + \varepsilon \tag{1}$$

where $y \in R^M$ is the available measurements, $\theta \in R^N$ is the unknown vector to be reconstructed, $X \in R^{M \times N}$ ($M < N$) is referred to as the sensing matrix, and ε is the error associated with the measurement noise. The unknown vector θ could be obtained by minimizing the following least-squares loss function

$$\widehat{\theta}_{LS} = \arg \min_{\theta} \|X\theta - y\|_2^2 \tag{2}$$

In order to obtain a unique and reasonable solution to this underdetermined problem, a regularization term is introduced to the objective function as

$$\widehat{\theta}_{L_p} = \arg \min_{\theta} \|X\theta - y\|_2^2 + \beta \|\theta\|_p^p \tag{3}$$

where β is the regularization parameter and $\|\cdot\|_p$ $(p \geq 0)$ is the p-norm. The l_1 regularization $(p = 1)$ and l_2 regularization $(p = 2)$ take the following forms, respectively, as

$$\widehat{\boldsymbol{\theta}}_{L_1} = \arg\min_{\widehat{\boldsymbol{\theta}}} \ \|\boldsymbol{X}\boldsymbol{\theta} - \boldsymbol{y}\|_2^2 + \beta_1\|\boldsymbol{\theta}\|_1 \tag{4}$$

$$\widehat{\boldsymbol{\theta}}_{L_2} = \arg\min_{\widehat{\boldsymbol{\theta}}} \ \|\boldsymbol{X}\boldsymbol{\theta} - \boldsymbol{y}\|_2^2 + \beta_2\|\boldsymbol{\theta}\|_2^2 \tag{5}$$

where $\beta_1, \beta_2 > 0$. The elastic net method combines the l_1 and l_2 regularization techniques as follows

$$\widehat{\boldsymbol{\theta}}_{EN} = \arg\min_{\widehat{\boldsymbol{\theta}}} \ \|\boldsymbol{X}\boldsymbol{\theta} - \boldsymbol{y}\|_2^2 + \beta_1\|\boldsymbol{\theta}\|_1 + \beta_2 \|\boldsymbol{\theta}\|_2^2 \tag{6}$$

where $\beta_1\|\boldsymbol{\theta}\|_1 + \beta_2 \|\boldsymbol{\theta}\|_2^2$ is referred to as the elastic net penalty, which is a convex combination of the l_1 and l_2 regularization terms and thus has the characteristics of both l_1 and l_2 regularization techniques. When $1 < p < 2$ in Equation (3), although the corresponding regularization techniques have many similarities with the elastic net, they cannot produce sparse solutions. It has been proved mathematically that among all regularization techniques with $p \geq 1$, only the l_1 regularization favors sparsity in the solution [35].

The elastic net problem in Equation (6) can be transformed into an equivalent l_1 regularization problem on augmented data [34], and thus can promote sparsity in the solution similar to the l_1 regularization technique. Moreover, the elastic net method fixes the problem of the l_1 regularization in terms of grouped variables. As shown in Equations (4)-(6), the elastic net and l_2 regularization penalties are strictly convex, while the l_1 regularization penalty is convex but not strictly. Strictly convex penalty functions guarantee the grouping effect that they have the ability of identifying grouped variables simultaneously. Details of the proof can be found in Reference [34].

If the sensing matrix $\boldsymbol{X}$ is assumed to be orthogonal, i.e., $\boldsymbol{X}^T\boldsymbol{X} = \boldsymbol{I}$, the solutions of the l_1 and l_2 regularizations and elastic net can be expressed as follows [34]

$$\widehat{\boldsymbol{\theta}}_{L_1,i} = \left(\left|\widehat{\boldsymbol{\theta}}_{LS,i}\right| - \frac{\beta_1}{2}\right)_+ \cdot \text{sgn}\left(\widehat{\boldsymbol{\theta}}_{LS,i}\right) \tag{7}$$

$$\widehat{\boldsymbol{\theta}}_{L_2} = \frac{1}{1+\beta_2}\widehat{\boldsymbol{\theta}}_{LS} \tag{8}$$

$$\widehat{\boldsymbol{\theta}}_{EN,i} = \frac{1}{1+\beta_2} \cdot \left(\left|\widehat{\boldsymbol{\theta}}_{LS,i}\right| - \frac{\beta_1}{2}\right)_+ \cdot \text{sgn}\left(\widehat{\boldsymbol{\theta}}_{LS,i}\right) \tag{9}$$

where the subscript i denotes the ith item, and $(\cdot)_+$ denotes the positive part of the respective argument. According to Equations (7)-(9), the elastic net can be viewed as a two-step procedure, i.e., a direct shrinkage from the l_2 regularization followed by a soft thresholding due to the l_1 regularization. Consequently, the elastic net incurs a double shrinkage, and thus introduces an extra bias compared with the pure l_1 or l_2 regularization technique. To this end, a scaling transformation is conducted to undo shrinkage in order to improve the prediction accuracy of the elastic net. Let $\boldsymbol{\theta}_{EN}^* = (1+\beta_2)\boldsymbol{\theta}_{EN}$, then the corrected elastic net estimates are given by [34]

$$\widehat{\boldsymbol{\theta}}_{EN}^* = \arg\min_{\boldsymbol{\theta}} \boldsymbol{\theta}^T \left(\frac{\boldsymbol{X}^T\boldsymbol{X} + \beta_2\boldsymbol{I}}{1+\beta_2}\right)\boldsymbol{\theta} - 2\boldsymbol{y}^T\boldsymbol{X}\boldsymbol{\theta} + \beta_1\|\boldsymbol{\theta}\|_1 \tag{10}$$

The objective function for the l_1 regularization in Equation (4) can be rewritten as

$$\widehat{\boldsymbol{\theta}}_{L_1} = \arg\min_{\boldsymbol{\theta}} \boldsymbol{\theta}^T (\boldsymbol{X}^T\boldsymbol{X})\boldsymbol{\theta} - 2\boldsymbol{y}^T\boldsymbol{X}\boldsymbol{\theta} + \beta_1\|\boldsymbol{\theta}\|_1 \tag{11}$$

Comparing Equations (10) and (11), the key difference between the elastic net and l_1 regularizations lies in the added term $\beta_2\boldsymbol{I}$. Through adding a small value on the diagonal items of $\boldsymbol{X}^T\boldsymbol{X}$, the condition number of $\boldsymbol{X}^T\boldsymbol{X}$ can be reduced significantly. According to the sparse recovery theory, the more well-conditioned the Gram matrix (i.e., $\boldsymbol{X}^T\boldsymbol{X}$) is, the better the l_1 regularization recovers the unknown sparse vector [21]. Therefore, the elastic net can be regarded as a stabilized version of the l_1 regularization technique.

In summary, the elastic net algorithm works as well as the l_1 regularization technique in terms of enforcing sparsity in the solution, and fixes the problems of stability and grouping.

3. Damage Identification using the Elastic Net Algorithm

3.1 Sensitivity-based model updating

The stiffness matrix of a structure can be modeled as follows

$$K = \sum_{i=1}^{n} \alpha_i K^i \tag{12}$$

where K^i is the ith element stiffness matrix, α_i is the associated stiffness parameter, and n is the number of elements in the finite element (FE) model. Existing damage detection methods usually assume that only the element stiffness parameter reduces to $\tilde{\alpha}_i$ when damage occurs, and the mass and damping remain unchanged. The stiffness reduction factor (SRF) is then defined as [22]

$$p_i = \frac{\tilde{\alpha}_i - \alpha_i}{\alpha_i} \tag{13}$$

The SRF is chosen as the damage parameter in this study, which indicates both damage location and damage severity.

Sensitivity-based model updating is to find changes in structural model parameters through minimizing the discrepancy between analytical and measured structural properties [36]. According to the Taylor series expansion, the relationship between the damage parameters p and change in the modal parameters ΔR can be linearly expressed as [37]

$$S \cdot p = \Delta R = R^E - R^0 \tag{14}$$

where R^E and R^0 are the measured and initial analytical modal parameters, respectively, and S is the sensitivity matrix of the modal parameters with respect to the damage parameters.

In this study, natural frequencies and mode shapes are utilized for damage detection. Therefore, the modal parameters and sensitivity matrix consist of two parts as

$$R = \begin{bmatrix} R_\lambda \\ R_\phi \end{bmatrix} \tag{15}$$

$$S = \begin{bmatrix} S_\lambda \\ S_\phi \end{bmatrix} \tag{16}$$

where $\boldsymbol{\lambda}$ and $\boldsymbol{\phi}$ are eigenvalues and mode shapes, respectively. $\boldsymbol{R}_\lambda$ and $\mathbf{S}_\lambda$ can be expressed as

$$\boldsymbol{R}_\lambda = [\lambda_1, \lambda_2, \cdots, \lambda_m]^T \tag{17}$$

$$\mathbf{S}_\lambda = \left[\mathbf{S}_{\lambda_1}, \mathbf{S}_{\lambda_2}, \cdots, \mathbf{S}_{\lambda_m}\right]^T \tag{18a}$$

$$\mathbf{S}_{\lambda_i} = \frac{\partial \lambda_i}{\partial \boldsymbol{p}} = \left\{\frac{\partial \lambda_i}{\partial p_1}, \frac{\partial \lambda_i}{\partial p_2}, \cdots, \frac{\partial \lambda_i}{\partial p_n}\right\} \tag{18b}$$

where λ_i is the ith eigenvalue and m is the number of measured modes. $\boldsymbol{R}_\phi$ and $\mathbf{S}_\phi$ can be expressed as

$$\boldsymbol{R}_\phi = \left[\boldsymbol{R}_{\phi_1}, \boldsymbol{R}_{\phi_2}, \cdots, \boldsymbol{R}_{\phi_m}\right]^T \tag{19a}$$

$$\boldsymbol{R}_{\phi_i} = \left[\phi_{1,i}, \phi_{2,i}, \cdots, \phi_{np,i}\right]^T \tag{19b}$$

$$\mathbf{S}_\phi = \left[\mathbf{S}_{\phi_1}, \mathbf{S}_{\phi_2}, \cdots, \mathbf{S}_{\phi_m}\right]^T \tag{20a}$$

$$\mathbf{S}_{\phi_i} = \frac{\partial \boldsymbol{\phi}_i}{\partial \boldsymbol{p}} = \begin{bmatrix} \dfrac{\partial \phi_{1,i}}{\partial p_1} & \dfrac{\partial \phi_{1,i}}{\partial p_2} & \cdots & \dfrac{\partial \phi_{1,i}}{\partial p_n} \\ \dfrac{\partial \phi_{2,i}}{\partial p_1} & \dfrac{\partial \phi_{2,i}}{\partial p_2} & \cdots & \dfrac{\partial \phi_{2,i}}{\partial p_n} \\ \vdots & \vdots & \ddots & \vdots \\ \dfrac{\partial \phi_{np,i}}{\partial p_1} & \dfrac{\partial \phi_{np,i}}{\partial p_2} & \cdots & \dfrac{\partial \phi_{np,i}}{\partial p_n} \end{bmatrix} \tag{20b}$$

where $\phi_{j,i}$ is the ith mode shape at the jth point and np is the number of measurement points. $\mathbf{S}$ can be calculated either from the global FE model [38] or using the substructuring approach [39]. According to Equations (16), (18) and (20), adjacent elements cause similar changes in structural modal parameters, and thus the adjacent columns of $\mathbf{S}$ are linearly dependent. Therefore, $\mathbf{S}$ is ill-conditioned with a large condition number. As introduced in Section 2, the elastic net method is able to improve the condition of the sensitivity matrix through including the l_2 regularization term, and is thus well suitable for the sensitivity-based model updating.

3.2 Iterative damage identification via the elastic net

Since the relationship between the modal parameters $\boldsymbol{R}$ and damage parameters $\boldsymbol{p}$ is nonlinear, the Gauss-Newton method is employed to calculate the damage parameters

through an iterative procedure. For the kth iteration model updating,

$$\mathbf{S}^{k-1} \cdot \Delta \mathbf{p}^k = \Delta \mathbf{R}^{k-1} \tag{21}$$

where

$$\mathbf{S}^{k-1} = \mathbf{S}\left(\sum_{i=1}^{k-1} \Delta \mathbf{p}^i\right) = \frac{\partial \mathbf{R}\left(\sum_{i=1}^{k-1} \Delta \mathbf{p}^i\right)}{\partial \mathbf{p}} \tag{22}$$

$$\Delta \mathbf{R}^{k-1} = \mathbf{R}^E - \mathbf{R}\left(\sum_{i=1}^{k-1} \Delta \mathbf{p}^i\right) \tag{23}$$

The superscript $(k-1)$ denotes the results calculated from the $(k-1)$th iteration. The iteration is terminated upon the following convergence criterion is met

$$\frac{\|\Delta \mathbf{p}^k\|_2}{\left\|\sum_{i=1}^{k} \Delta \mathbf{p}^i\right\|_2} \leq Tol \tag{24}$$

The damage parameters after kth iterations are thus obtained as

$$\mathbf{p}^k = \sum_{i=1}^{k} \Delta \mathbf{p}^i \tag{25}$$

According to Equations (1), (10) and (21), the damage parameters at the kth iteration $\Delta \mathbf{p}^k$ can be calculated by solving the below optimization problem using the elastic net algorithm

$$\Delta \hat{\mathbf{p}}^k = \arg \min_{\Delta \hat{\mathbf{p}}^k} (\Delta \mathbf{p}^k)^T \left[\frac{(\mathbf{S}^{k-1})^T \mathbf{S}^{k-1} + \beta_2 \mathbf{I}}{1 + \beta_2}\right] \Delta \mathbf{p}^k - 2(\Delta \mathbf{R}^{k-1})^T \mathbf{S}^{k-1} \Delta \mathbf{p}^k + \beta_1 \|\Delta \mathbf{p}^k\|_1 \tag{26}$$

Two regularization parameters, β_1 and β_2, need to be determined in the elastic net. They control the contributions of l_1 regularization and l_2 regularization to the overall optimization problem. Zuo and Hastie [34] determined the two regularization parameters through the cross validation (CV) on a two-dimensional surface. A small grid of values for β_2 is first formulated, i.e. $(0, 0.01, 0.1, 1, 10, 100)$. For each β_2, β_1 is then determined using the CV method. Finally, β_2 is selected as the one with the smallest residual of the CV function.

As shown in Equation (26), for a small β_2, the ill-conditioned problem of the sensitivity matrix cannot be solved effectively. By contrast, a large β_2 will place a high penalty on the

l_2 regularization term, leading to an over-smooth solution. Zuo and Hastie [34] showed that the optimization result was sensitive to β_1 rather than β_2 as only a coarse grid of values for β_2 was required. In this regard, β_2 is fixed as 0.01 in this study in order to reduce the computation burden, and β_1 is determined by examining the residual and solution norms [40]. The following numerical and experimental studies show that satisfactory damage identification results can be obtained when $\beta_2 = 0.01$ for different damage scenarios (DSs).

The proposed damage identification procedure is summarized below:

1. Initialize $\boldsymbol{\alpha}^0$, $\boldsymbol{S}^0$, and $\Delta \boldsymbol{R}^0$.

2. At the $(k-1)$th iteration,

    Calculate $\Delta \boldsymbol{p}^{k-1}$ using Equation (26);

    Update $\boldsymbol{S}^{k-1}$ and $\Delta \boldsymbol{R}^{k-1}$ using Equations (22) and (23).

3. Repeat step 2 for the kth iteration until the following convergence criterion is met

$$\frac{\|\Delta \boldsymbol{p}^k\|_2}{\left\|\sum_{i=1}^k \Delta \boldsymbol{p}^i\right\|_2} \leq Tol$$

4. A Numerical Example

4.1 Model description

A cantilever beam (Figure 1) is first utilized as a preliminary numerical study. The total length of the beam is 1.0 m, and the cross-section area is 5.0×49.6 mm^2. The mass density and Young's modulus are 7.67×10^3 kg/m^3 and 2.0×10^{11} N/m^2, respectively. The beam is modeled with 100 equal Euler–Bernoulli beam elements (i.e., $n = 100$), each 10 mm long. The damage is simulated by the reduction of the bending stiffness with the mass remaining unchanged. To examine the grouping effect of the proposed method, elements 1 and 2 close to the clamped end are damaged by 50%, that is, SRF(1) = SRF(2) = −0.5 and all other

SRF = 0.
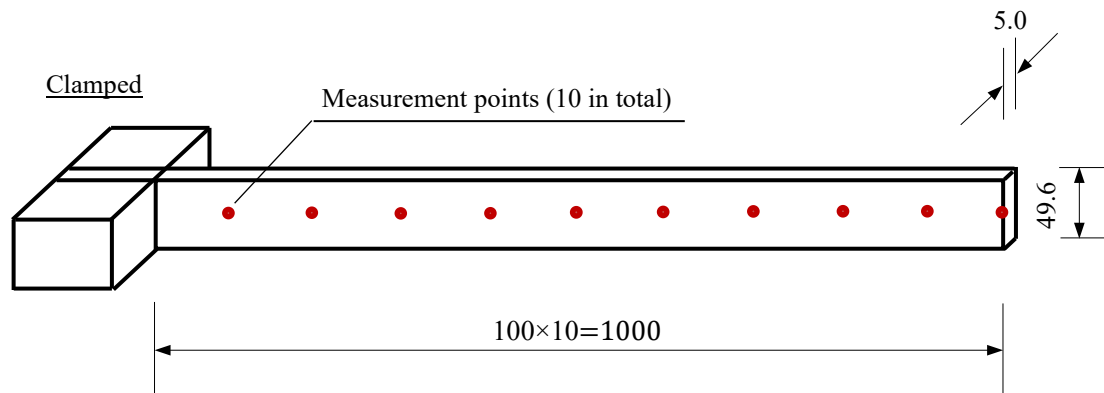
Figure 1 Geometric configuration of the beam structure (Unit: mm)

4.2 Damage detection

The mode shapes at 10 points are assumed to be available in the undamaged and damaged states, which are chosen every 100 mm (Figure 1). The natural frequencies and modal assurance criterion (MAC) of the undamaged and damaged structures are compared in Table 1. The simulated damage only causes a small change in MAC, while relatively large changes in natural frequencies. To investigate the effect of measurement noise on the damage detection accuracy, two different levels of noise will be introduced into the modal parameters in the damaged state. For noise level 1, normal distributed random noises with zero mean and standard deviation of 1% and 5% of the real data are respectively added to the frequencies and mode shapes. For noise level 2, the standard deviation of the frequencies and mode shapes increases to 2% and 10% of the real data, respectively.

Table 1 Modal data of the beam model in the undamaged and damaged states

Mode no.	Undamaged	Damaged		
		No noise	Noise level 1	Noise level 2

	Freq. (Hz)	Freq. (Hz)	MAC	Freq. (Hz)	MAC	Freq. (Hz)	MAC
1	3.53	3.40 (–3.69)	1.000	3.41 (–3.68)	1.000	3.46 (–2.03)	1.000
2	21.92	21.22 (–3.17)	0.999	21.03 (–4.06)	0.998	21.27 (–2.95)	0.995
3	61.23	59.46 (–2.88)	0.997	59.47 (–2.87)	0.998	59.93 (–2.11)	0.995
4	118.40	115.24 (–2.67)	0.995	117.98 (–0.36)	0.996	117.28 (–0.95)	0.993
5	195.34	191.02 (–2.21)	0.993	192.75 (–1.32)	0.992	191.71 (–1.86)	0.988
6	294.77	288.89 (–1.99)	0.992	289.83 (–1.68)	0.992	292.08 (–0.91)	0.989
Average		(–2.77)	0.996	(–2.33)	0.996	(–1.80)	0.993

Note: Values in parentheses are the frequency change ratios (%) between the damaged and undamaged states.

4.2.1 Using noise-free modal data

The first six natural frequencies and the associated mode shapes without noise are first used for damage identification. The initial stiffness parameters are set at their nominal values $p^0 = \{0, ... ,0\}^T$, indicating that no damage is present. The convergence criterion for the iteration process is set as *Tol* = 0.001. The regularization parameter is determined as $\beta_1 = 0.02$.

In each iteration, the damage parameters are obtained by minimizing Equation (26). The condition number of the initial Gram matrix is as large as $\text{cond}(S^T S) = 2.24 \times 10^{20}$. Through including the l_2 regularization term, the condition number of the Gram matrix is reduced significantly as $\text{cond}(S^T S + \beta_2 I) = 24.85$. Consequently, the ill-conditioned problem of the sensitivity-based damage detection is resolved, and a stable solution could be obtained. The iterative identification process converges after 3 iterations only, as shown in Figure 2. In the first iteration, damaged elements 1 and 2 are identified, and no false identification occurs. However, the identified damage severities differ much from the true values. As the iteration proceeds, the identified damage parameters tend to approach the actual values, and the two adjacent damaged elements are located and quantified accurately.
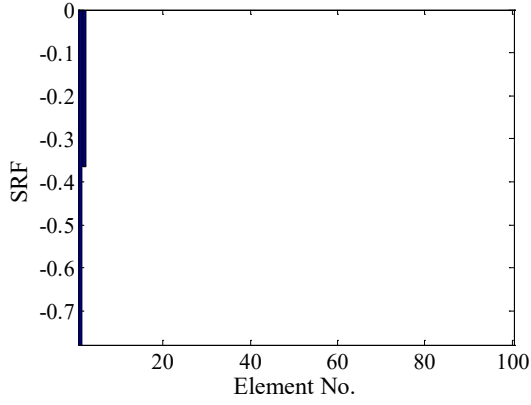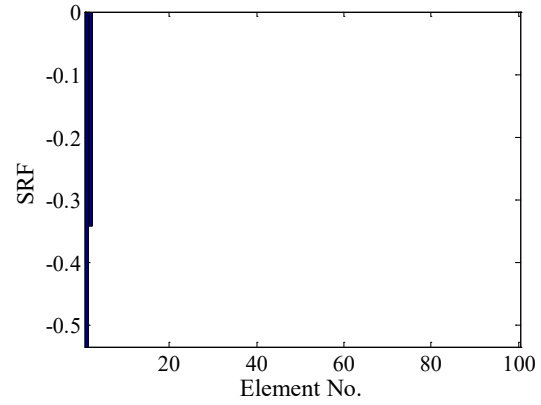
(a) Iteration No. 1
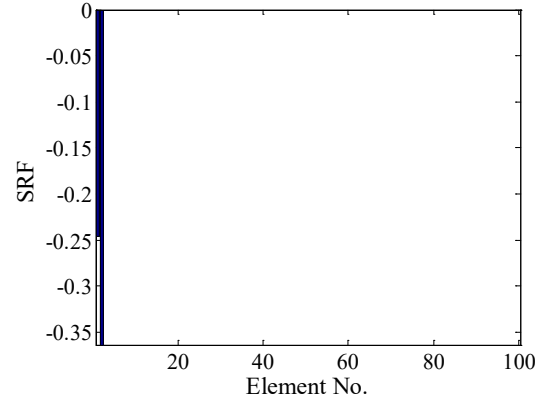
(b) Iteration No. 2
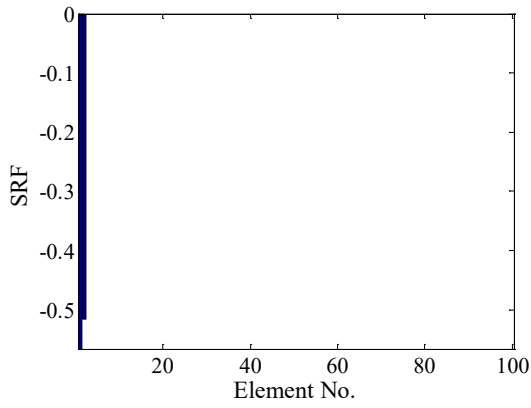
(c) Iteration No. 3

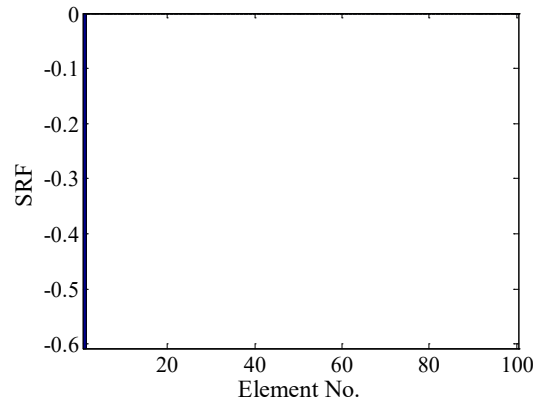Figure 2 Damage identification results during the iterative process (no noise)

The l_1 regularization technique [22] is also employed here for comparison purpose. The following objective function is minimized for damage identification in each iteration

$$\Delta \widehat{\boldsymbol{p}}^k = \arg \min_{\Delta \widehat{\boldsymbol{p}}^k} \| \boldsymbol{S}^{k-1} \Delta \boldsymbol{p}^k - \Delta \boldsymbol{R}^{k-1} \|_2^2 + \beta_1 \| \Delta \boldsymbol{p}^k \|_1 \qquad (28)$$

The regularization parameter is determined as $\beta_1 = 0.07$ based on the residual and solution norms [40]. The identification results are shown in Figure 3. The damaged element 1 is correctly identified but element 2 is not. This indicates that only one of the grouped damages but not all can be detected.
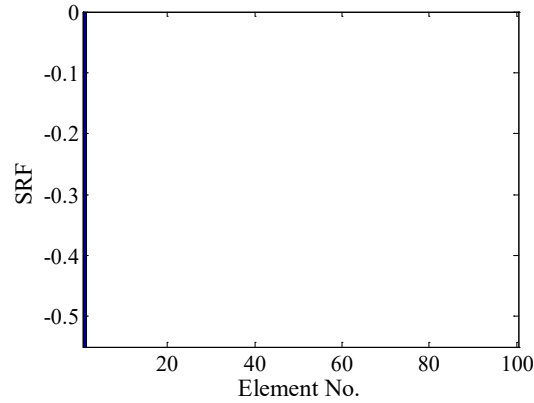
Figure 3 Damage identification result with the l_1 regularization technique (no noise)

4.2.2 Using modal data of noise level 1

For noise level 1, the noisy modal data are used for damage detection, and Equation (26) is similarly solved. The regularization parameters are the same as those using noise-free modal data. The damage parameters during the iteration process are shown in Figure 4. After four iterations, the actually damaged elements are correctly detected, although the SRF of element 2 has a small error. The damage identification result using the l_1 regularization technique is shown in Figure 5. Similar to the above result, the l_1 regularization method can only identify one of the two damaged elements.
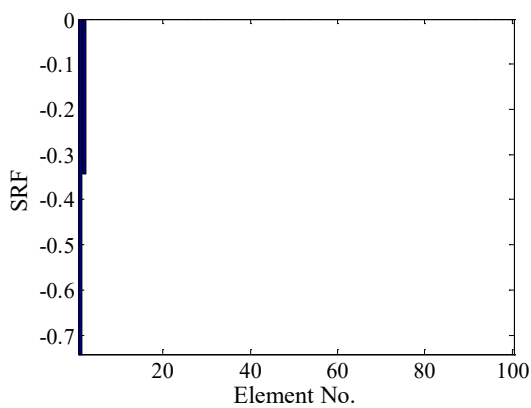
(a) Iteration No. 1
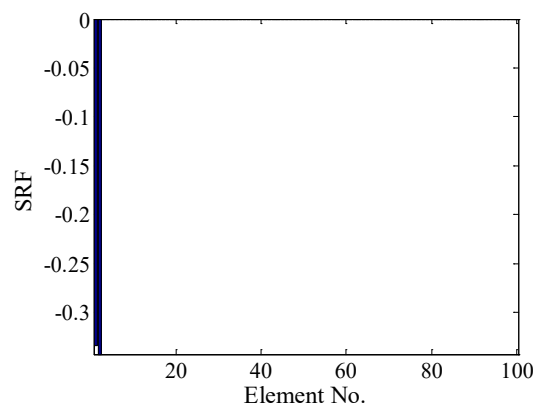
(b) Iteration No. 2
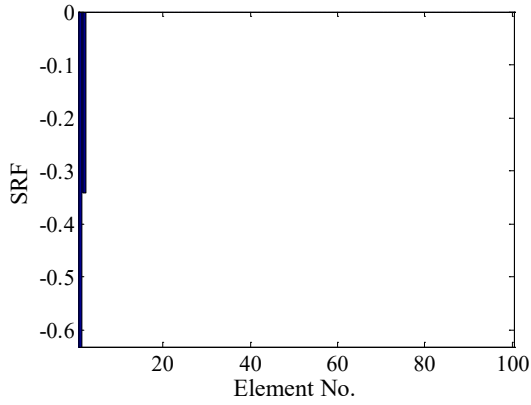
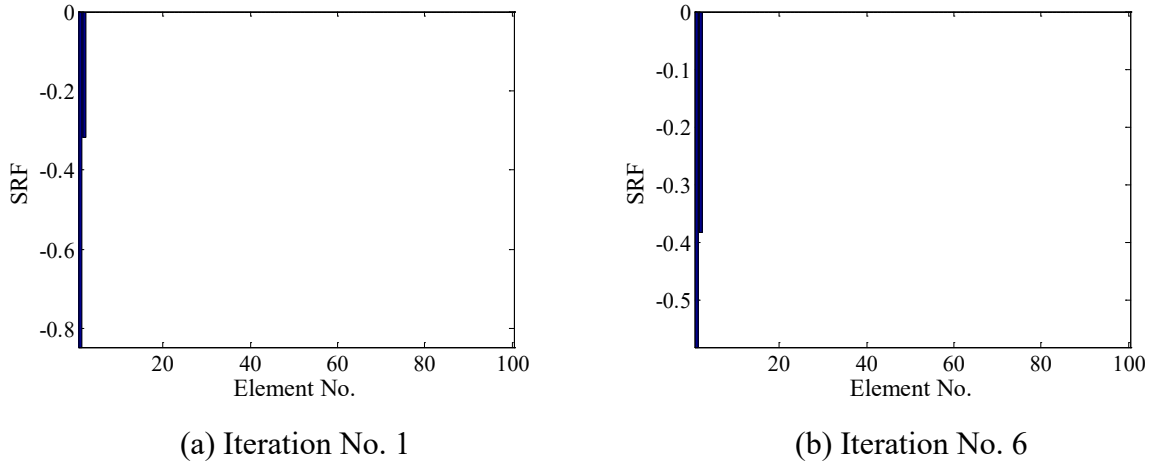(c) Iteration No. 3   (d) Iteration No. 4

Figure 4 Damage identification results during the iterative process (noise level 1)

Figure 5 Damage identification result with the l_1 regularization technique (noise level 1)

4.2.3 Using modal data of noise level 2

In the case of noise level 2, the regularization parameters are the same as those using noise-free modal data. The damage identification process converges after 6 iterations, and only the results in the first and last iterations are displayed in Figure 6 for brevity. The two adjacent damaged elements are identified accurately. As shown in Figure 7, the l_1 regularization technique can only detect one of the grouped damages.

(a) Iteration No. 1   (b) Iteration No. 6

Figure 6 Damage identification results during the iterative process (noise level 2)
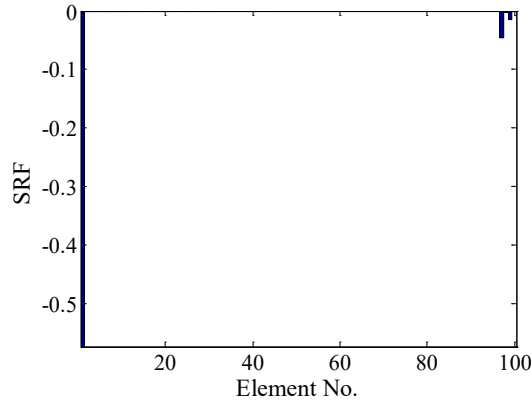
Figure 7 Damage identification result with the l_1 regularization technique (noise level 2)

The identification error and computation time of the elastic net technique are compared with those using the l_1 regularization technique in Table 2. The identification error is defined as

$$\delta = \sqrt{\frac{\|\boldsymbol{p} - \overline{\boldsymbol{p}}\|_2^2}{n}} \qquad (29)$$

where $\overline{\boldsymbol{p}}$ denotes the actual damage parameters. In both damage detection methods, the corresponding objective functions (26) and (28) are minimized using Optimization Toolbox in MATLAB [41], in which the active-set method is employed. The calculations are carried out on a PC with Intel Core i7 3.60 GHz CPU and 16 GB RAM.

The computation time of the elastic net technique is slightly longer than that of the l_1 regularization, while the damage identification error of the former is much smaller than the latter. For both techniques, more iterations are required for convergence when using the noisy modal data. The elastic net method is able to identify the grouped damage correctly even at a high noise level.

The above numerical results show that the elastic net method is effective in locating and quantifying grouped structural damage, whilst the l_1 regularization technique can only identify one damaged element from the group. Moreover, the proposed method has good robustness to noise.

Table 2 Comparison of damage detection results of the cantilever beam

Algorithm		Iteration No.	Identification error	Time consumption
Noise-free	Elastic net	3	0.63%	17.74 sec
	L_1 regularization	3	5.02%	14.00 sec
Noise level 1	Elastic net	4	2.61%	21.65 sec
	L_1 regularization	4	5.11%	16.62 sec
Noise level 2	Elastic net	6	2.18%	32.67 sec
	L_1 regularization	6	5.08%	27.99 sec

5. An Experimental Example

5.1 Model descriptions

The experimental example is a three-story steel frame that was presented in Hou et al. [22]. The geometric dimensions of the frame are shown in Figure 8. The beams and columns have the same cross-section dimension as $75.0 \times 5.0 \ mm^2$. The mass density and Young's modulus

of the frame are 7.92×10^3 kg/m^3 and 2.0×10^{11} N/m^2, respectively.

The frame was excited with an instrumented hammer with a rubber tip. The direction and location of the excitation point are shown in Figure 8. Bruel & Kjaer accelerometers with a magnetic base were firmly mounted on the frame to measure the acceleration responses. The signals were conditioned and amplified through a Bruel & Kjaer 2962 amplifier, then collected by the Kyowa EDX-100A data acquisition system. The instruments are shown in Figure 9.
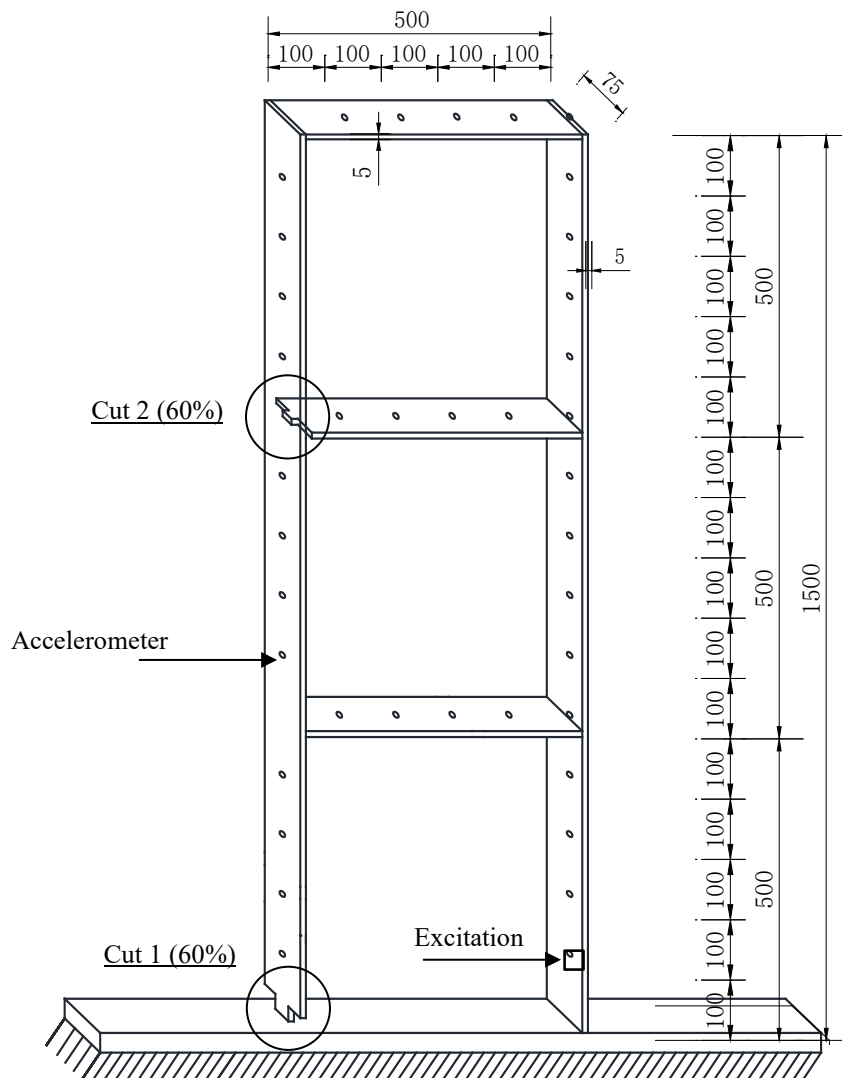
Figure 8 Overview of the frame structure (Unit: mm)

(a) Signal amplifier (Bruel & Kjaer 2962)

(b) Data acquisition box (EDX-100A)

(c) Hammer (SINOCERA LC-04A)

Figure 9. Experiment instrumentation

The sampling frequency of the test was 2000 Hz since the frequency range of interest is 0~100 Hz. In order to obtain the complete mode shapes of the whole frame, the measurement points were chosen every 100 mm. Due to the high axial stiffness, the horizontal responses of the points on the beam are identical. Therefore, 39 measurement points as illustrated in Figure 8 were selected. For the measurement points on the beam and columns, the horizontal and vertical accelerations were measured, respectively. Since only nine accelerometers were available (Figure 10), five set-ups were tested, in which additional masses with the same weight as the accelerometers were employed as the dummy sensors. In each set-up, the structure was impacted eight times for the purpose of averaging, and each impact lasted for 30 seconds. The frequency response function of each measurement point was then calculated. Afterwards, the accelerometers roved along the frame and swapped with the dummy sensors

to keep the mass of the frame unchanged. The hammer's impacting location and direction remained unchanged for different set-up. Finally the measured frequency response functions of all 39 measurement points were combined, and the complete mode shapes of the frame were calculated using the rational fraction polynomial method [42].
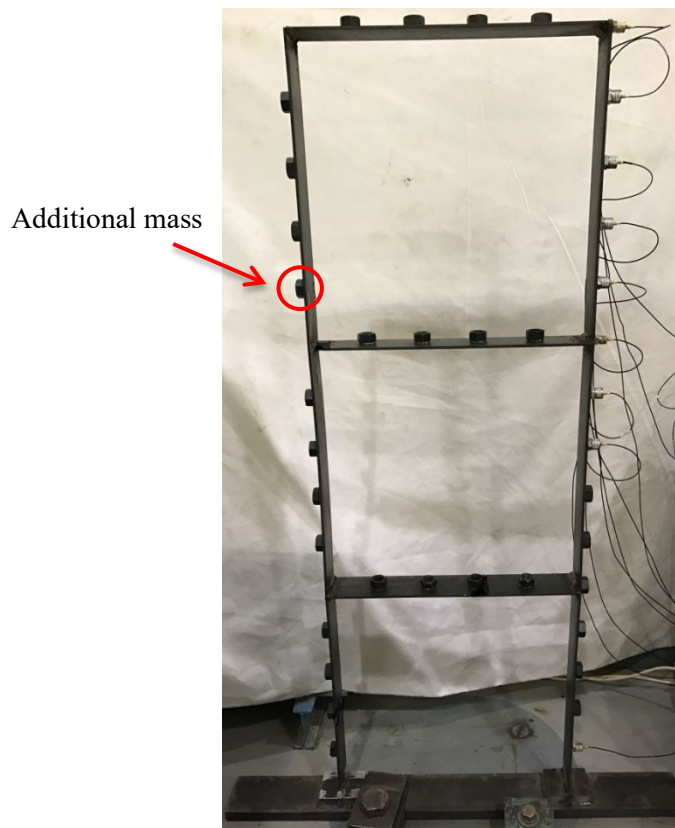

Figure 10 Layout of accelerometers and added mass

Two saw cuts were sequentially introduced into the frame model, corresponding to two DSs (Figure 8). Cuts 1 and 2 are located at the bottom of the column and the beam-column joint, respectively. The saw cuts have the same length $b = 20$ mm and depth $d = 22.5$ mm, and thus the moment of inertia of the cut sections are reduced by 60%. The modal testing was conducted on the intact frame and then repeated for two damage states. The first eight frequencies and mode shapes, as listed in Table 3, were extracted and used for damage detection. The measured frequencies and mode shapes of the frame in the undamaged state are illustrated in Figure 11.

Table 3 The measured modal data of the frame in the undamaged and damaged states

Mode	Undamaged	DS1		DS2	
no.	Freq. (Hz)	Freq. (Hz)	MAC	Freq. (Hz)	MAC
1	4.23	4.13 (−2.31)	92.02	4.08 (−3.53)	95.78
2	14.03	13.75 (−1.96)	99.02	13.45 (−4.11)	97.49
3	25.45	25.14 (−1.19)	98.87	25.13 (−1.23)	99.01
4	44.81	44.70 (−0.23)	94.74	44.69 (−0.27)	97.59
5	58.12	57.39 (−1.24)	92.45	57.28 (−1.44)	91.46
6	68.36	67.34 (−1.49)	93.01	66.11 (−3.29)	88.14
7	72.27	72.06 (−0.28)	96.30	71.42 (−1.18)	85.80
8	91.73	89.14 (−2.83)	86.79	88.51 (−3.52)	76.38
Average		(−1.44)	94.15	(−2.32)	91.46

Note: Values in parentheses are the frequency change ratios (%) between the damaged and undamaged states.
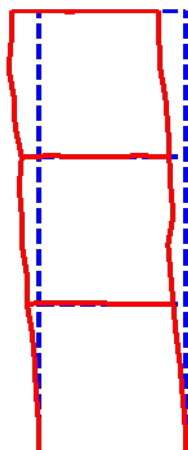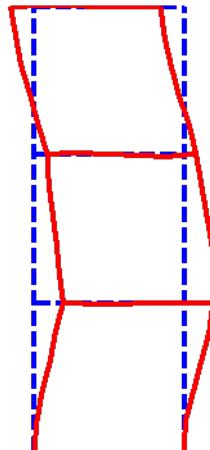
Mode 1 (4.23 Hz) Mode 2 (14.03 Hz) Mode 3 (25.45 Hz)
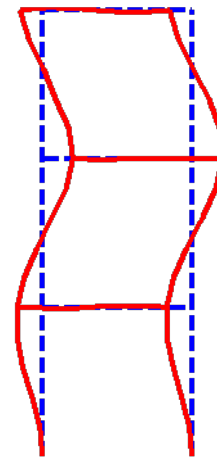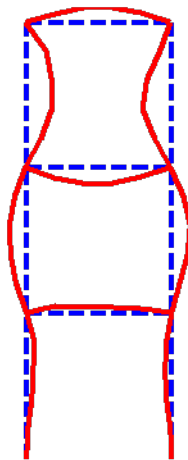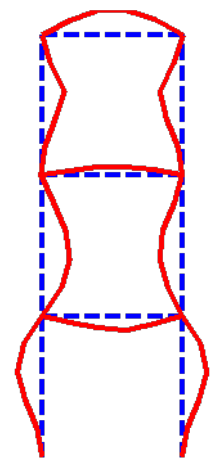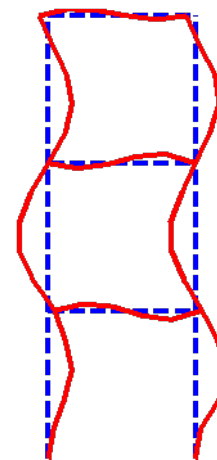
Mode 4 (44.81 Hz) Mode 5 (58.12 Hz) Mode 6 (68.36 Hz)

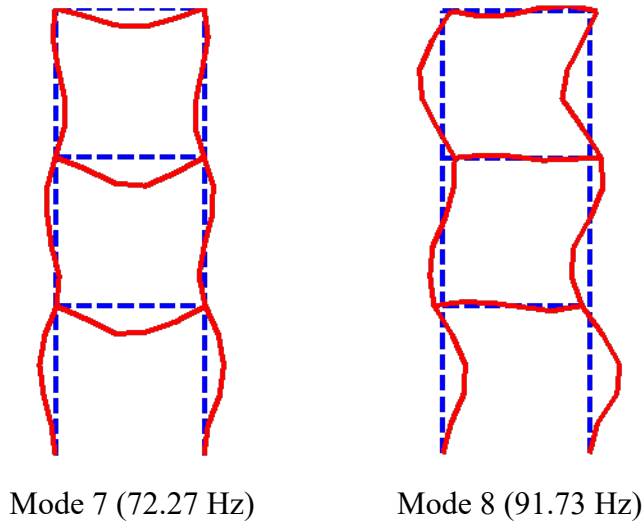Mode 7 (72.27 Hz)   Mode 8 (91.73 Hz)

Figure 11 The measured mode shapes of the frame in the undamaged state

5.2 FE modeling of the frame

Two FE modeling schemes are employed in this study to investigate the effectiveness of the proposed damage identification algorithm. In the first scheme, the frame is divided into 225 elements, each 20 mm long. Cuts 1 and 2 are located at elements 1 and 176, respectively. As the length of one element is identical to that of each cut, the damage severity equals to the reduction in the moment of inertia of the cut section, that is, $SRF(1) = SRF(176) = -60\%$.

To examine the effectiveness of the proposed method in identifying grouped variables, the frame is also modeled with 450 elements (each 10 mm long) in the second FE modeling scheme, in which each cut corresponds to two damaged elements since the length of each cut is double that of one element. Table 4 lists the damage locations and severities of the two DSs in both schemes. The FE models have two and four damaged elements, which are extremely sparse compared to the total 225 and 450 elements, respectively.

The initial FE model is updated using the experimental data in the undamaged state to reduce the influence of modeling errors of the initial FE model. No regularization is employed in this step. The updated FE model can represent the structure more accurately, as its modal

properties match the measured ones of the structure, which will be used for damage detection in the next section.

Table 4 Damage locations and severities for the two DSs

FE model	DS1	DS2
Scheme 1 ($n = 225$)	SRF(1) = −60%	SRF(1) = −60%
		SRF(176) = −60%
Scheme 2 ($n = 450$)	SRF(1) = −60%	SRF(1) = −60%
	SRF(2) = −60%	SRF(2) = −60%
		SRF(351) = −60%
		SRF(352) = −60%

5.3 Damage detection

The first eight natural frequencies and the associated mode shapes are used for damage identification. As the numerical example, the initial damage parameters $\boldsymbol{p}^0 = \{0, \ldots, 0\}^T$ and the convergence criterion is $Tol = 0.001$.

5.3.1 Damage detection using FE modeling scheme 1

When the first FE modeling scheme is used, there are 312 measurement data and 225 unknown SRF values to be identified, which is an over-determined problem. The regularization parameters for DS1 and DS2 are determined as $\beta_1 = 0.3$ and $\beta_1 = 0.2$, respectively. Following the iterative procedures summarized in Section 3, the damage parameters in the two DSs are obtained and displayed in Figures 12 and 13. In order to display the results more clearly, enlarged figures corresponding to the damaged area are also provided. For DS1, the damage parameters converge after two iterations only. The damage location and severity are identified accurately and no false identification occurs. For DS2, the process converges after 7 iterations, and only the results in the first and last iterations are shown for brevity. The two damaged elements are accurately detected.
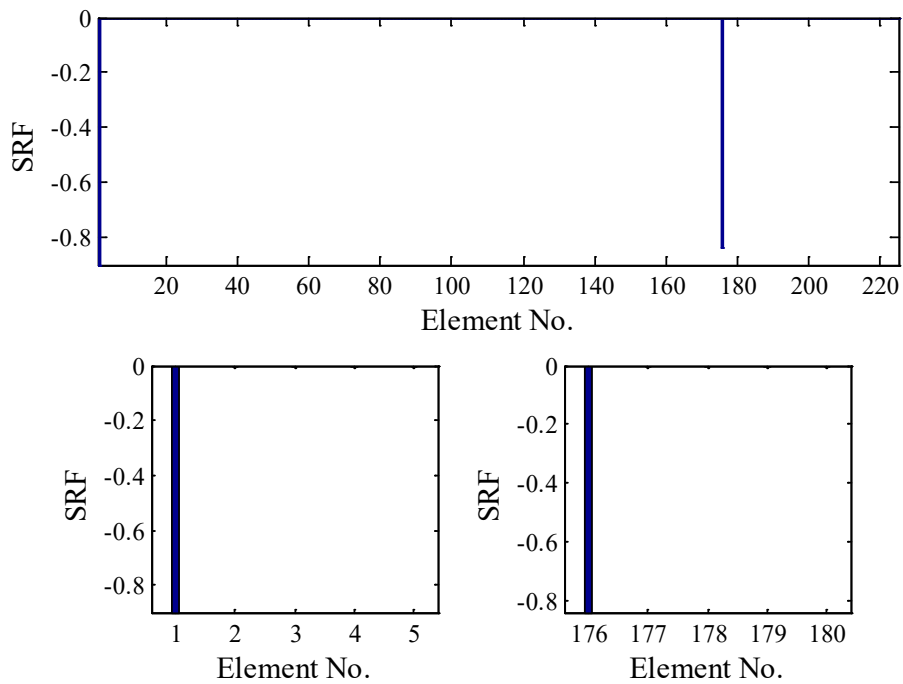
24
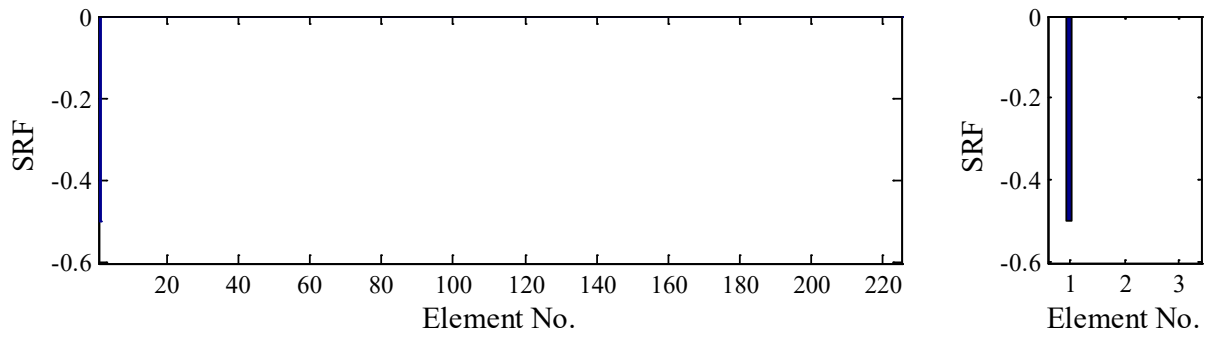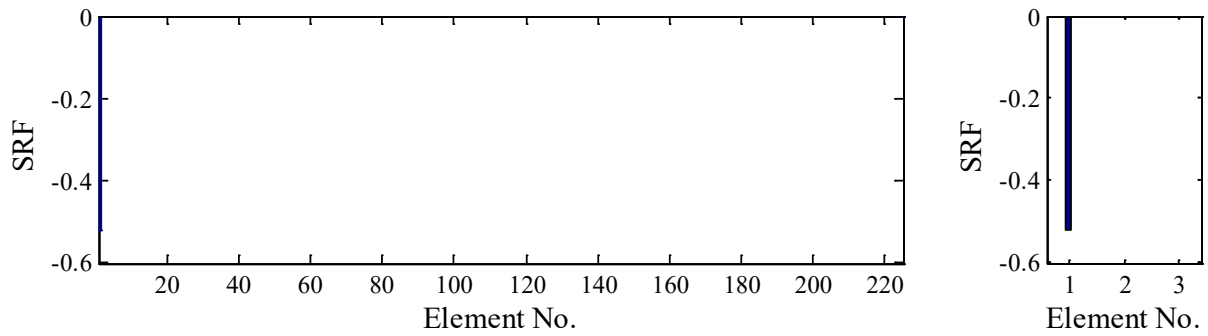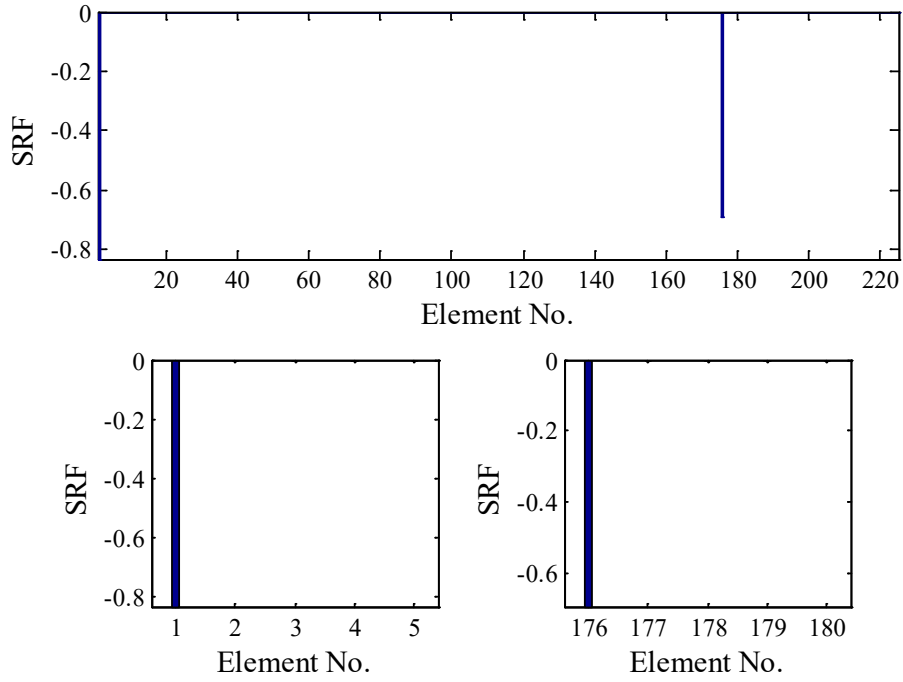
(a) Iteration No. 1

(b) Iteration No. 2

Figure 12 Damage identification results during the iterative process for DS1
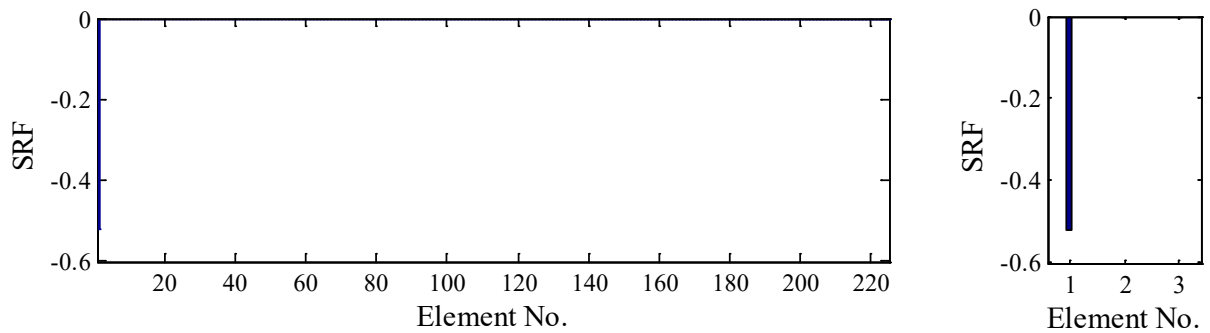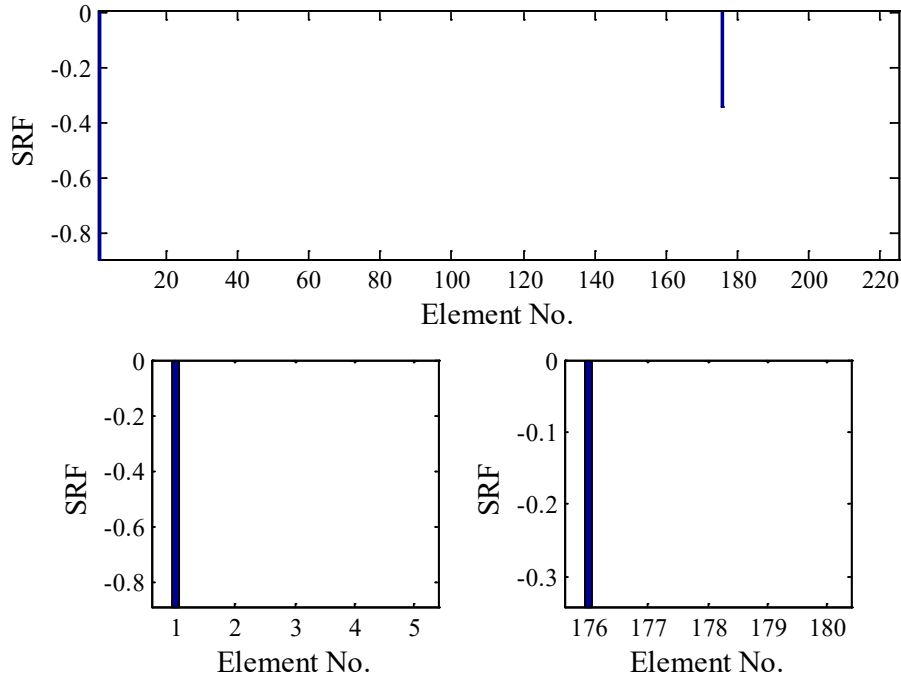

(a) Iteration No. 1

(b) Iteration No. 7

Figure 13 Damage identification results during the iterative process for DS2

The damage identification results with the l_1 regularization technique are shown in Figure 14. For DS1, the damaged element is detected with a good accuracy. For DS2, the two damage locations are identified correctly and no false identification occurs. However, the SRF of Element 176 has a large error.
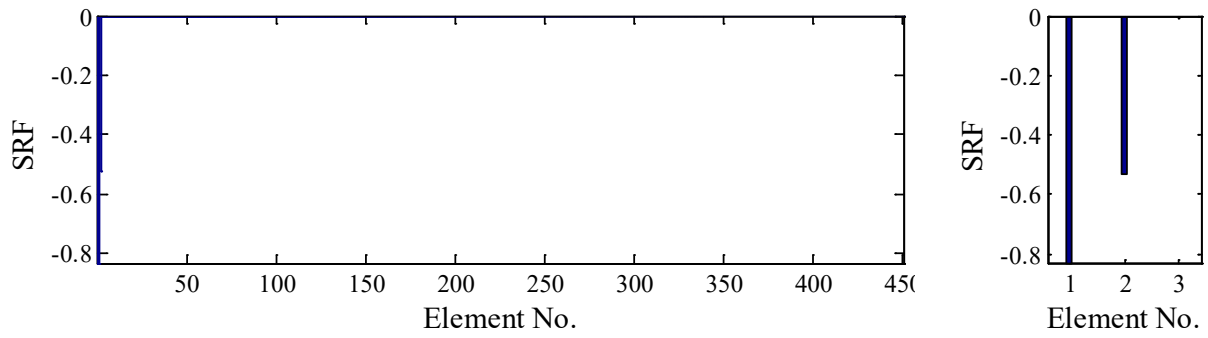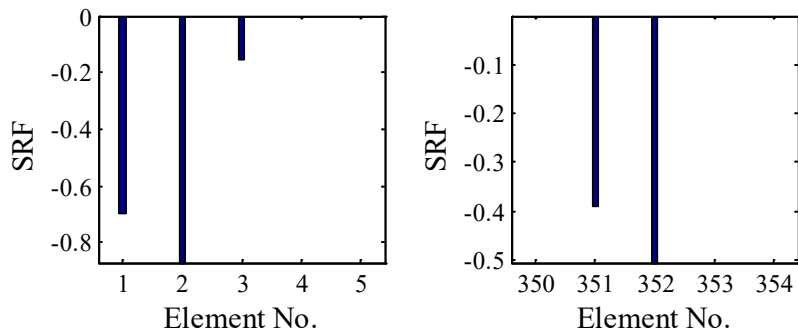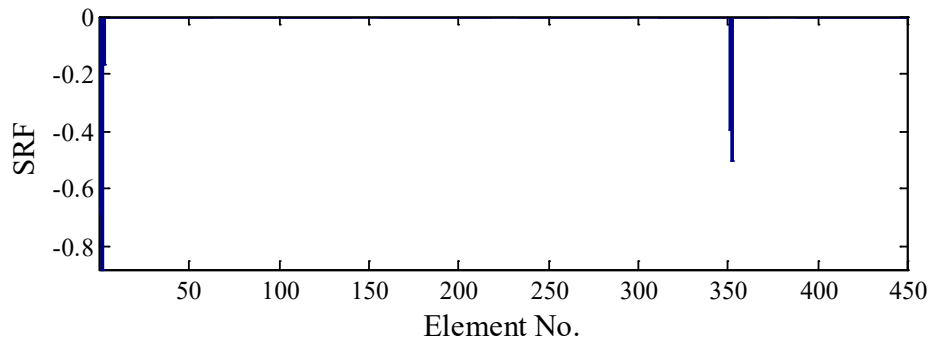

(a) DS1

(b) DS2

Figure 14 Damage identification results with the l_1 regularization technique

5.3.2 Damage detection using FE modeling scheme 2

When FE modeling scheme 2 is used, it has 450 unknown SRF values to be identified whereas there are 312 measurement data, which is an underdetermined problem. The regularization parameters for DS1 and DS2 are determined as $\beta_1 = 0.1$ and $\beta_1 = 0.15$, respectively. The identification results for DS1 and DS2 are shown in Figure 15. For DS1, the results converge and the two adjacent damaged elements are accurately detected after two iterations. In DS2, two groups of elements (1, 2, 351 and 352) were damaged. The convergence is achieved after four iterations, and all four damaged elements are accurately detected upon convergence, although the SRF of Element 3 has a small error.
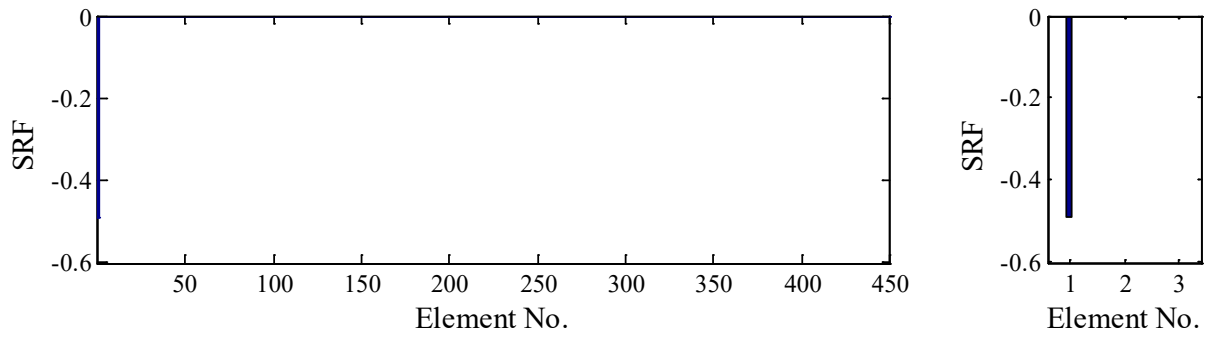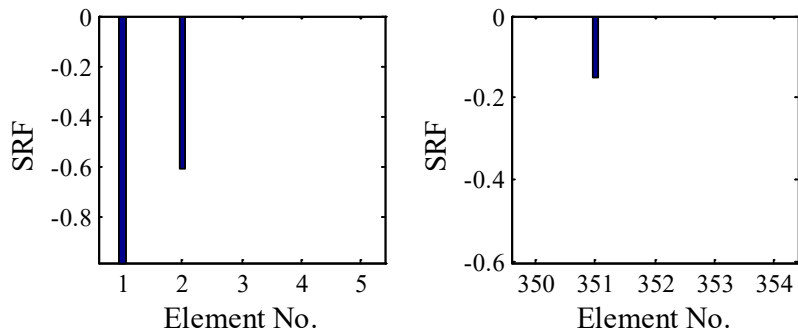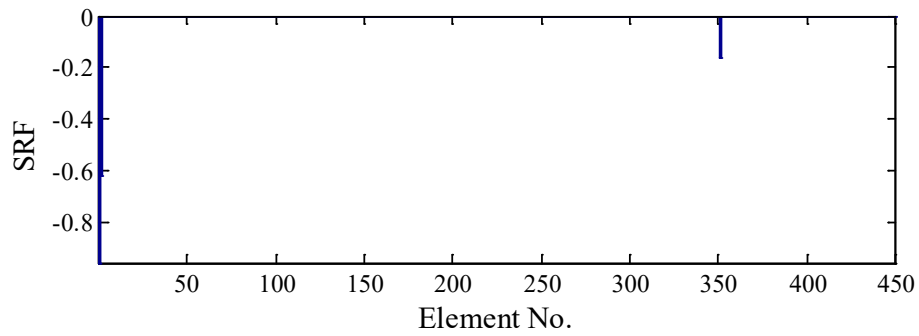
27

(a) DS1

(b) DS2

Figure 15 Damage identification results using the second FE modeling scheme

The damage identification results with the l_1 regularization technique are shown in Figure 16. For DS1, only one of the two damaged elements can be detected. In DS2, only the first 2 damaged elements in Cut 1 can be identified accurately.

(a) DS1

(b) DS2

Figure 16 Damage identification results using the second FE modeling scheme with the l_1 regularization technique

The damage detection results with the l_1 regularization and the proposed methods are compared in Table 5. In both DSs, the two methods consumed similar computation time, while the proposed elastic net method is able to obtain more accurate identification results than the l_1 regularization technique.

Table 5 Comparison of damage detection results using elastic net and l_1 regularization technique

	Algorithms	Elastic net	L_1 regularization
DS1	Identification error	1.13%	2.88%
	Time consumption	9.46 min	8.66 min
DS2	Identification error	1.93%	3.81%
	Time consumption	8.67 min	9.50 min

The example demonstrates that the developed method is able to identify grouped structural damage, whereas the l_1 regularization cannot. Consequently, with the proposed damage detection method, the length of the element in the FE model can be shorter, and thus finer damaged elements can be detected

6. Conclusions and Discussions

A sparse damage identification method has been proposed in this study using natural frequencies and mode shapes. The nonlinear sensitivity-based model updating is linearized through an iterative procedure. The elastic net method is employed to identify the sparse damage, which exploits the advantages of both l_1 and l_2 regularization techniques. The proposed method is able to enforce sparsity in the solution as the l_1 regularization technique does. Through including the l_2 regularization term, the condition of the sensitivity matrix and thus the robustness and stability of the method are improved. Moreover, the proposed method enables the grouped structural damage being identified simultaneously.

Numerical and experimental examples verify that the proposed sparse damage detection technique can identify single and multiple damages accurately. The examples also demonstrate that the elastic net method is able to successfully detect grouped structural damage, even when the number of measurement data is much less than the number of

elements, which is advantageous over the l_1 regularization technique. Therefore, the structure of interest can be modeled with a larger number of elements using the proposed method, such that smaller local damage can be directly modeled and quantified.

Acknowledgements

References

1. Salawu OS. Detection of structural damage through changes in frequency: a review. *Eng Struct* 1997; 19(9): 718–723.

2. Li J, Hao H, Xia Y, et al. Damage Detection of Shear Connectors in Bridge Structures with Transmissibility in Frequency Domain. *Int J Struct Stab Dyn* 2014; 14(2): 1350061.

3. Chen C and Yu L. A hybrid ant lion optimizer with improved Nelder–Mead algorithm for structural damage detection by improving weighted trace lasso regularization. *Adv Struct Eng* 2020; 23(3): 468–484.

4. Doebling SW, Farrar CR, Prime MB, et al. Damage identification and health monitoring of structural and mechanical systems from changes in their vibration characteristics: a literature review, *Los Alamos National Laboratory Report*, 1996.

5. Sohn H, Farrar CR, Hemez FM, et al. A review of structural health monitoring literature: 1996–2001, *Los Alamos National Laboratory Report*, 2003.

6. Esfandiari A, Nabiyan MS and Rofooei FR. Structural damage detection using principal component analysis of frequency response function data. *Struct Health Monit* 2020; 27(7): e2550.

7. Zhang FL, Kim CW and Goi Y. Efficient Bayesian FFT method for damage detection using ambient vibration data with consideration of uncertainty. *Struct Control Health Monit* 2021; 28: e2659.

8. Ghoulem K, Kormi T and Bel Hadj Ali N. Damage detection in nonlinear civil structures using kernel principal component analysis. *Adv Struct Eng* 2020 23(11): 2414–2430

9. Guo T, Wu LP, Wang CJ, et al. Damage detection in a novel deep-learning framework: a robust method for feature extraction. *Struct Health Monit* 2020; 19(2): 424–442.

10. Padil KH, Bakhary N, Abdulkareem M, et al. Non-probabilistic method to consider uncertainties infrequency response function for vibration-based damagedetection using Artificial Neural Network. *J Sound Vib* 2020; 467: 115069.

11. Beheshti Aval SB, Ahmadian V, Maldar M, et al. Damage detection of structures using signal processing and artificial neural networks. *Adv Struct Eng* 2020; 23(5): 884–897

12. Kullaa J. Robust damage detection in the time domain using Bayesianvirtual sensing

with noise reduction and environmental effectelimination capabilities. *J Sound Vib* 2020; 473: 115232.

13. Wah WSL, Chen YT, Owen JS. A regression-based damage detection method for structures subjected to changing environmental and operational conditions. *Eng Struct* 2021; 228: 111462.

14. Bao YQ, Chen ZC, Wei SY, et al. The state of the art of data science and engineering in structural health monitoring. *Eng* 2019; 5(2): 234–242.

15. Sun LM, Shang ZQ, Xia Y, et al. Review of bridge structural health monitoring aided by big data and artificial intelligence: from condition assessment to damage detection, *J Struct Eng* 2020; 146(5): 04020073.

16. Hou RR and Xia Y. Review on the new development of vibration-based damage identification for civil engineering structures: 2010-2019. *J Sound Vib* 2021; 491: 115741.

17. Li X and Law SS. Adaptive Tikhonov regularization for damage detection based on nonlinear model updating. *Mech Syst Signal Process* 2010; 24(6): 1646–1664.

18. Weber B, Paultre P and Proulx J. Structural damage detection using nonlinear parameter identification with Tikhonov regularization. *Struct Control Health Monit* 2007; 14(3): 406–427.

19. Tikhonov AN and Arsenin VY. *Solutions of Ill-Posed Problems*, Wiley, New York, 1977.

20. Hansen VY. Analysis of discrete ill-posed problems by means of the L-curve. *SIAM Rev* 1992; 34(4): 561–580.

21. Theodoridis S, Kopsinis Y and Slavakis K. Sparsity-aware learning and compressed sensing: an overview. *Acad Press Libr Singnal Process* 2013; 1271–1377.

22. Hou RR, Xia Y and Zhou XQ. Structural damage detection based on l_1 regularization using natural frequencies and mode shapes. *Struct Control Health Monit* 2018; 25(3): e2107.

23. Ding ZH, Li J and Hao H. Structural damage identification by sparse deep belief network using uncertain and limited data. *Struct Control Health Monit* 2020; 27(5): e2522.

24. Yang YC and Nagarajaiah S. Structural damage identification via a combination of blind

feature extraction and sparse representation classification. *Mech Syst Signal Process* 2014; 45(1): 1–23.

25. Liu HL, Yu L, Luo ZW, et al. Multi-strategy structural damage detection based on included angle of vectors and sparse regularization. *Struct Eng Mech* 2020; 75(4): 415–424.

26. Hernandez EM. Identification of isolated structural damage from incomplete spectrum information using l_1-norm minimization. *Mech Syst Signal Process* 2014; 46(1): 59–69.

27. Zhang C, Huang JZ, Song GQ, et al. Structural damage identification by extended Kalman filter with l_1-norm regularization scheme. *Struct Control Health Monit* 2017; 24(11): e1999.

28. Yuan M and Lin Y. Model selection and estimation in regression with grouped variables. *J R Stat Soc Series B* 2006; 68(1): 49–67.

29. Grave E, Obozinski GR and Bach FR. Trace lasso: a trace norm regularization for correlated designs. In: *Proc Advances Neural Inform Process Syst*, 2011, pp.2187–2195.

30. Zuo WM, Meng DY, Zhang L, et al. A generalized iterated shrinkage algorithm for non-convex sparse coding. In: *Proceedings of IEEE International Conference on Computer Vision (ICCV)*, Sydney, Australia, 3–6 December 2013, pp.217–224.

31. Tibshirani R. Regression shrinkage and selection via the lasso. *J R Statist Soc B* 1996; 58(1): 267–288.

32. Fu W. Penalized regression: the bridge versus the lasso. *J Computnl Graph Statist* 1998; 7(3): 397–416.

33. Xu H, Caramanis C and Mannor S. Sparse algorithms are not stable: A no-free-lunch theorem. *IEEE PAMI* 2012; 34(1): 187–193.

34. Zou H and Hastie T. Regularization and variable selection via the elastic net. *J R Statist Soc B* 2005; 67(2): 301–320.

35. Candès EJ, Wakin M and Boyd S. Enhancing sparsity by reweighted l_1 minimization. *J Fourier Anal Appl* 2008; 14(5): 877–905.

36. Bakir PG, Reynders E and De Roeck G. Sensitivity-based finite element model updating using constrained optimization with a trust region algorithm. *J Sound Vib* 2007; 305(1):

211–225.

37. Zhou XQ, Xia Y and Weng S. L_1 regularization approach to structural damage detection using frequency data. Struct Health Monit 2015; 14(6): 571–658.

38. Nelson RB. Simplified calculation of eigenvector derivatives. AIAA J 1976; 4(9): 1201–1205.

39. Weng S, Xia Y, Xu YL, et al. An iterative substructuring approach to the calculation of eigensolution and eigensensitivity. *J Sound Vib* 2011; 330(14): 3368–3380.

40. Hou RR, Xia Y, Bao YQ, et al. Selection of regularization parameter for l_1-regularized damage detection. J Sound Vib 2018; 423: 141–160.

41. MATLAB. Optimization toolbox user's guide,version 3. Natick, MA: The Mathworks Inc., 2005.

42. Formenti D and Richardson M. Parameter estimation from frequency response measurements using rational fraction polynomials (twenty years of progress). Proceedings of International Modal Analysis Conference, Orlando, Florida, 2002, 167–181.